THE JOURNAL OF PHYSICAL CHEMISTRY C

Article

Understanding the Active Sites of CO Hydrogenation on Pt-Co Catalysts Prepared Using Atomic Layer Deposition

Joseph A. Singh, Nuoya Yang, Xinyan Liu, Charlie Tsai, Kevin H Stone, Bart Johnson, Ai Leen Koh, and Stacey F. Bent

J. Phys. Chem. C, **Just Accepted Manuscript** • DOI: 10.1021/acs.jpcc.7b10541 • Publication Date (Web): 22 Dec 2017

Just Accepted

ACS Publications

The Journal of Physical Chemistry C is published by the American Chemical Society. 1155 Sixteenth Street N.W., Washington, DC 20036

Understanding the Active Sites of CO Hydrogenation on Pt-Co Catalysts Prepared Using Atomic Layer Deposition

Joseph A. Singh,[†] Nuoya Yang, [‡] Xinyan Liu,[§] Charlie Tsai, [§] Kevin H. Stone,[‖] Bart Johnson,[‖] Ai Leen Koh,[¶] and Stacey F. Bent,[§]*

† Department of Chemistry, Stanford University, 333 Campus Drive, Stanford, California, 94305, United States

‡ Department of Materials Science and Engineering, Stanford University, 496 Lomita Mall, Stanford, California, 94305, United States

§ Department of Chemical Engineering, Stanford University, 443 Via Ortega, Stanford, California, 94305, United States

‖ SSRL, SLAC National Accelerator Laboratory, Menlo Park, California, 94025, United States

¶ Stanford Nano Shared Facilities, Stanford University, 476 Lomita Mall, Stanford, California, 94305, United States

ABSTRACT

The production of liquid fuels and industrial feedstocks from renewable carbon sources is an ongoing scientific challenge. Using atomic layer deposition together with conventional techniques, we synthesize Pt-Co bimetallic catalysts that show improvement for syngas conversion to alcohols. By combining reaction testing, *x-ray* diffraction, electron microscopy, and *in situ* infrared spectroscopy experiments, supported by density functional theory calculations, we uncover insights into how Pt modulates the selectivity of Co catalysts. The prepared Pt-Co catalysts demonstrate increased selectivity towards methanol and low molecular weight hydrocarbons as well as a modest increase in selectivity towards higher alcohols. The *in situ* infrared spectroscopic measurements suggest that these changes in selectivity result from an interplay between linear and bridging carbon monoxide configurations on the catalyst surface.

TEXT

Introduction:

Supply instability and environmental concerns of fossil fuels have led to increasing interest in fuels and industrial feedstocks originating from nonpetroleum and renewable sources. The Fischer-Tropsch process allows for the conversion of syngas, a mixture of hydrogen and carbon monoxide, to hydrocarbon products according to the Anderson–Schulz–Flory distribution,[1] with a small production of oxygenates. Current catalyst technology offers poor performance for the conversion of syngas to oxygenates, with the exception of methanol.

Methanol, ethanol, and other linear alcohols are attractive both as a feedstock for making commodity chemicals and as fuel additives. Currently there are no catalysts for the production of higher alcohols from syngas that meet the requirements of activity and selectivity for large scale

production. In the case of Fischer-Tropsch-based catalysts, previous work has shown that the addition of transition metal promoters can increase oxygenate production by cobalt catalysts.[2–9] The addition of platinum in particular has been shown to increase the selectivity of cobalt catalysts towards oxygenates.[4,10,11] However, the mechanism for enhanced oxygenate production remains unresolved on the Pt-Co system, for which comparatively few mechanistic studies have been performed compared to CuZn, CuCo, MoS_2, and other oxygenate synthesis catalysts.

In the present study, we investigate cobalt Fischer-Tropsch catalysts functionalized with Pt grown by atomic layer deposition (ALD). We compare the results with alloy catalysts prepared using traditional synthetic methods. Previous work on platinum-promoted cobalt Fischer-Tropsch catalysts focused on catalysts prepared using traditional wet synthetic methods such as incipient wetness impregnation (IWI).[4,12–16] Compared to impregnation synthesis, ALD offers advantages for catalytic studies[17–22] including the uniform coating of high surface area substrates, low impurity incorporation, enhanced performance, and creation of nanostructured catalysts. In this study, we exploit these properties to create novel CO hydrogenation catalysts from Co promoted by surface Pt nanoclusters. Taking advantage of ALD's high degree of control, we systematically promote Co/SiO_2 catalysts using Pt deposited with ALD. Given ALD's low deposition temperature and mild gas phase chemistry, the technique allows for the creation of series of catalysts with similar dispersion, surface area, and other materials properties allowing for direct comparison in a controlled environment. We compare these catalysts with those prepared using IWI. One previous study examined the use of ALD Pt as a promoter of Co catalysts for increased activity under Fischer-Tropsch conditions.[23] That study prepared catalysts using ALD of both Co_3O_4 and Pt and compared with IWI preparation.[23] The use of Pt in both cases was found to improve activity over that of pure Co-based catalysts; however, IWI was

found to be more effective for increasing the activity.[23] In this work, we focus on changes in catalyst selectivity and utilize *in situ* spectroscopic measurements to understand how different surface CO binding configurations correlate with the observed selectivity changes.

Our prepared catalysts show increased selectivity toward methanol, short chain hydrocarbons, and higher alcohols from gas phase CO hydrogenation, and the changes are well-correlated with surface structural changes measured using real time *in situ* diffuse reflectance infrared Fourier transform spectroscopy (DRIFTS). We utilize density functional theory (DFT) calculations to support our experimental results. We demonstrate that the addition of platinum to cobalt catalysts using ALD improves selectivity towards oxygenates while decreasing selectivity towards longer chain hydrocarbon products. We propose as an explanation for this result that the addition of Pt increases the amount of nondissociatively bound CO and disfavors hydrocarbon chain growth.

Methods:

Catalysts were synthesized using incipient wetness impregnation (IWI) with 10 wt% metal loading. In brief, silica gel (SiO_2, Davisil grade 643, Sigma Aldrich) was degassed under vacuum for 1 hour to below 10 mTorr. Metal salts $Co(NO_3)_2*6H_2O$ (Aldrich) and/or $H_2PtCl_6*nH_2O$ (Aldrich) were dissolved in deionized water. The metal salt solutions were slowly added while the support was kept at vacuum until the volume of added solution was equal to the support pore volume. After impregnation, samples were allowed to sit for at least 1 hour at vacuum and dried at room temperature. Samples were calcined in a tube furnace at 350 ˚C.

Platinum ALD was performed using a commercial reactor (Gemstar, Arradiance). Samples were cleaned using UV irradiation and ozone exposure prior to deposition. Platinum ALD was performed using $(MeCp)PtMe_3$ (STREM) and O_2 at 250 ˚C in exposure mode, in which the precursors are held in the reactor for a fixed time after pulsing. The Pt precursor was heated to 75

˚C. In each cycle, (MeCp)$PtMe_3$ was pulsed for 1 s and exposed for 60 s, (MeCp)$PtMe_3$ was purged for 180 s with nitrogen gas, oxygen was pulsed for 0.1 s and exposed for 60 s, and the oxygen was purged for 180 s with nitrogen gas. Powders were contained in custom stainless steel holders during the ALD process based upon design by Libera et al.[24] Catalysts with ALD coating will be referred to in shorthand, for example "10 cyc Pt/Co/SiO_2" for a catalyst with 10 cycles of Pt ALD performed on Co supported on silica gel.

Transmission electron microscopy (TEM) was performed using samples supported on ultrathin carbon on holey carbon copper TEM grids (Ted Pella). Samples were imaged at 200 keV using a FEI G2 F20 Tecnai TEM equipped with a Gatan Orius camera. Aberration-corrected TEM, and scanning transmission electron microscopy (STEM) was performed using a FEI Titan environmental transmission electron microscope (ETEM) operated at 300 keV in high vacuum mode. The microscope was equipped with a Gatan OneView camera. Annular dark field (ADF) STEM images are diffraction contrast limited due to the presence of differential pumping apertures that limit the incoherently scattered electron collection angle to 70 mrad on the FEI Titan ETEM.

Powder x-ray diffraction (XRD) was performed using beam line 7-2 as SSRL. Incident photon energy was 15.5 keV and a Pilatus 300k detector was used. The incidence angle of the sample was changed to maintain a sample angle of half the 2θ angle at the center of the detector. Prior to XRD, samples were reduced *ex situ* at 450 ˚C in 5% H_2/N_2. Samples were mounted on Si wafers and encapsulated in Kapton tape. Signal arising from support scattering was subtracted using a silica gel reference sample.

Catalyst samples were tested using an Altamira Benchcat system. CO was purified to remove metal carbonyl impurities (PALL Gaskleen ST). Samples were prepared in a packed bed with

glass wool holding the particles in place and glass beads to help preheat the gas packed above the sample in a ¼ inch OD glass lined stainless steel tube. Reduction was performed using a flow of 10 SCCM H_2 mixed with 90 SCCM He at 450 ˚C for 4 hours at atmospheric pressure. Testing was performed at 250 ˚C using 2:1 H_2:CO (90 SCCM total) at 20 bar pressure. Additional testing was performed using an Altamira Benchcat 4000HP reactor. Nitrogen was used as the inert gas and carbon monoxide was purified by passing through a 300 ˚C alumina bed on the Benchcat 4000HP. Products were detected using an online Agilent 7890B gas chromatograph-mass spectrometer. Hydrocarbon and oxygenate products were quantified using a flame ionization detector (FID). Conversions were calculated based on the detected products. Selectivities are given as carbon-weighted selectivities in which the product production is multiplied by the carbon count of the product to track CO economy.

Temperature-programmed reduction (TPR) and chemisorption were performed using an Altamira AMI 300 system. Prior to testing, samples were heated to 300 ˚C in Ar to dry the samples and remove volatile impurities. TPR was performed at 10 ˚C/minute and using 10% hydrogen in argon. Hydrogen consumption was measured using a thermal conductivity detector (TCD). After reduction, samples were titrated with CO using pulses delivered by a calibrated sampling loop. The CO consumption was measured using a TCD during each pulse.

IR spectroscopy via DRIFTS was performed in a Bruker Vertex 70 spectrometer with a liquid nitrogen-cooled HgCdTe (MCT) detector. Samples were loaded into a Praying Mantis DRIFTS chamber (Harrick) equipped with a water-cooled, high pressure, and high temperature reaction cell with ZnSe windows. The chamber was evacuated using a rotary vane vacuum pump and samples were reduced *in situ* using flowing H_2 at 450 ˚C prior to measurement. DRIFTS measurements were performed at low pressure under vacuum conditions. Carbon monoxide gas

was purified by passing through a 300 ˚C bed of gamma alumina to decompose nickel and iron carbonyl impurities. CO hydrogenation measurements were performed based on work by Kumar *et al*.[25] Samples were heated to 250 ˚C and exposed to flowing CO at 3.5 Torr until the surface CO adsorption signal reached a constant value as measured using the MCT detector. Subsequently, CO flow was stopped, H_2 flow initiated, and the measurement started. Data was processed using the spectrum of the catalyst after a complete CO hydrogenation cycle as the background for the Co-containing catalysts.

For inductively coupled plasma optical emission spectrometry (ICP-OES) and inductively coupled plasma mass spectrometry (ICP-MS) characterization, catalysts were dissolved in boiling aqua regia. The solutions were diluted with deionized water and syringe filtered (<0.5 μm) to remove residual particles from the insoluble support. High purity ICP standards were purchased from Aldrich and diluted to the appropriate concentrations. Measurements were performed either using a Thermo Fisher ICAP 6300 Duo View or Thermo Scientific* XSERIES 2 ICP-MS. Both systems are within their standard detection limits and provide comparable accuracy for the concentrations used in this study.

X-ray photoelectron spectroscopy (XPS) was performed using PHI 5000 Versaprobe II and II spectrometers with a monochromated Al k-alpha source. The powder samples were mounted on In foil (Aldrich) for the XPS measurements. Samples were charge neutralized during acquisition to correct for sample charging.

Nitrogen physiosorption measurements were performed using a Micromeritics 3 Flex instrument. The Brunauer–Emmett–Teller (BET) method was used to calculate surface areas and Barett–Joyner–Halenda (BJH) method was used to calculate pore size distributions.

Electronic potential energies were calculated with DFT performed with the Quantum ESPRESSO plane-wave code.[26] A plane-wave cutoff of 500 eV was used for all calculations and the Brillouin zone was sampled with a Monkhorst-Pack *k*-point grid.[27] A dipole correction was applied to all surfaces. The Bayesian Error Estimation Functional with van der Waals corrections,[28] BEEF-vdW, was employed, which includes a correction for van der Waals forces based on the vdW-DF2 functional.[29]

Adsorption energies were calculated by optimizing the atomic geometries with a BFGS line search algorithm and vibrational frequencies were computed using a finite difference approximation to the Hessian and subsequent diagonalization to find the normal modes, as implemented in the Atomic Simulation Environment.[30]

Results:

Structural characterization of the catalysts after synthesis was performed using both XRD and TEM. Figure 1 shows X-ray diffractograms for an IWI-synthesized Pt Co_3O_4 catalyst, ALD-modified Pt/Co_3O_4 catalysts prepared with 10 and 25 ALD cycles respectively, and a Co_3O_4 control sample. All catalysts were prepared on silica gel (SiO_2) supports and the elemental ratios of Pt/Co determined by ICP were 0.15 for the IWI Pt Co_3O_4 catalyst, 0.20 for the Pt/Co_3O_4 catalyst modified with 10 Pt ALD cycles, and 0.80 for the Pt/Co_3O_4 catalyst modified with 25 Pt ALD cycles. The XRD results confirm the presence of the Co_3O_4 phase in the Co_3O_4 control sample prepared by IWI synthesis, based on comparison with literature (PDF card 00-042-1467). After the addition of Pt to the IWI Co_3O_4 samples using ALD, the Co_3O_4 peaks remain unchanged. However, new peaks corresponding to metallic Pt (PDF card 00-004-0802) appear for the sample with high Pt mass loading (25 cycles ALD Pt). For samples with 10 or fewer ALD

Pt cycles of deposition, no Pt signal can be detected above the background level, likely because the small Pt crystallites and low mass loading do not generate enough signal. On the other hand, for the catalyst prepared using the coimpregnation of Co and Pt salts, the XRD data reveals a phase of Co_3O_4 symmetry with peaks shifted towards higher d values compared to the pure Co_3O_4 phase (**Figure** 1). This shift can be explained by the incorporation of Pt into the Co_3O_4 lattice resulting in expansion of the structure.

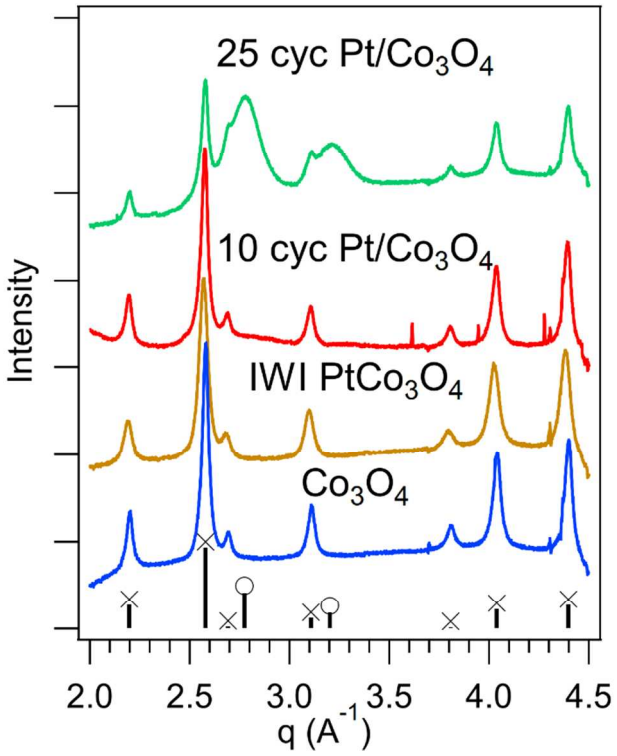

Figure 1. Powder x-ray diffraction of catalysts prior to reduction. The IWI Pt Co_3O_4 catalyst shows no Pt peaks and has peak shifts indicating lattice expansion. The 25 ALD Pt-modified catalyst shows peaks similar to those of the Co_3O_4/SiO_2 catalyst as well as peaks corresponding to metallic platinum. Lines at bottom are Co_3O_4 (crosses) and Pt (circles) reference structures (PDF cards 00-042-1467 and 00-004-0802, respectively).

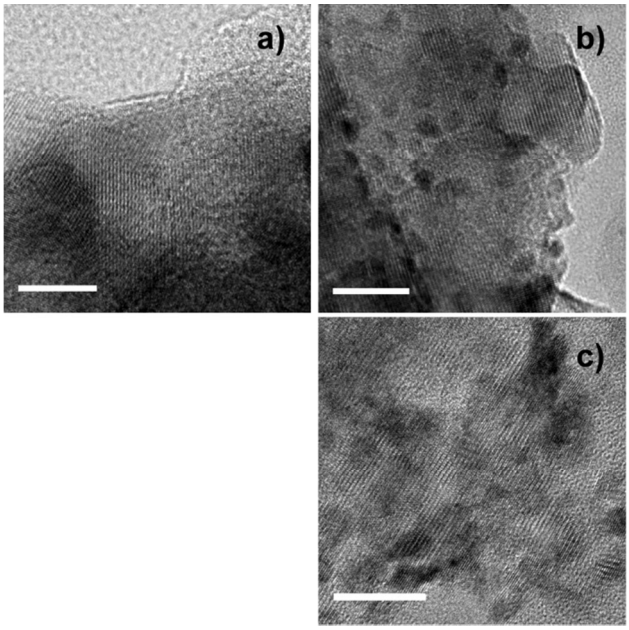

Figure 2. Bright-field TEM images of a) IWI Pt Co_3O_4/SiO_2, b) 10 cyc Pt/Co_3O_4/SiO_2, and c) 25 cyc ALD Pt/Co_3O_4/SiO_2 prior to reduction. The catalysts prepared using ALD show Pt nanoparticles. Scale bars are 10 nm.

Bright-field TEM micrographs of the IWI Pt Co_3O_4/SiO_2, 10 cyc Pt/Co_3O_4/SiO_2, and 25 cyc Pt/Co_3O_4/SiO_2 catalysts are presented in Figure 2. TEM of 10 cyc Pt/Co/SiO_2 catalyst prior to reduction (Figure 2b) shows fine dark, strongly diffracting (dark contrast) particles of less than 5 nm on the matrix, which correspond to a Pt phase with lattice fringes from a Co_3O_4 phase, in agreement with the bulk Pt and Co_3O_4 phases observed in XRD measurements. The 25 cyc Pt/Co_3O_4/SiO_2 catalyst (Figure 2c) shows both a higher coverage of and larger Pt particles. The TEM image of the IWI PtCo/SiO_2 catalyst (Figure 2a) does not show well-defined platinum particles, in contrast to catalysts with Pt provided using ALD. Combined with the XRD results, the TEM imaging hence indicates uniform incorporation of Pt into the IWI PtCo/SiO_2 catalyst structure.

X-ray diffractograms of the resulting catalysts after reduction (25 cyc Pt/Co/SiO_2, 10 cyc Pt/Co/SiO_2, IWI PtCo/SiO_2, and Co/SiO_2) are presented in Figure 3. After reduction, the Co_3O_4/SiO_2 catalyst is converted to metallic Co with FCC and HCP phases present (PDF cards 00-015-0806 and 01-071-4652). This agrees with prior work that showed cobalt Fischer-Tropsch catalysts contain a mixture of both FCC and HCP phases.[31] For low cycles of Pt ALD (10 or fewer) there is likewise the presence of FCC and HCP Co phases following reduction of the catalyst. The main peak near 3.1 A^{-1} is a convolution of the 002 peak of HCP Co and the 111 peak of FCC Co. Shifts in this peak can be explained by changes in the intensity ratios of the closely spaced HCP 002 and FCC 111 peaks for Co. No Pt peaks are observed for the 10 cycle sample which can be explained by small crystallite sizes and low mass loading as in the case prior to reduction. For the 25 cyc Pt/Co/SiO_2 catalyst, there is a broad feature with components corresponding to bulk Co and Pt phases as well as peaks due to the formation of a PtCo alloy phase with 1:1 stoichiometry (PDF card 01-071-7406). The powder diffraction scan of the IWI PtCo/SiO_2 catalyst after reduction shows a combination of FCC and HCP Co phases, similar to the case of the 10 cyc Pt/Co/SiO_2 catalyst, with no detectable Pt or alloy features. There may be a PtCo alloy phase present either as a minority component or a surface alloy that we are unable to detect using a bulk technique such as XRD. Post-reduction dark field STEM micrographs are presented in Figure 4 for the IWI PtCo/SiO_2 and 25 cyc Pt/Co/SiO_2 catalysts. The 25 cyc Pt/Co/SiO_2 sample shows fine bright particles corresponding to either Pt or Pt-rich domains, in agreement with the Pt features observed in the XRD measurements. Although the catalysts were exposed to air during sample preparation, we observe only metallic phases in the measurements performed after catalyst reduction.

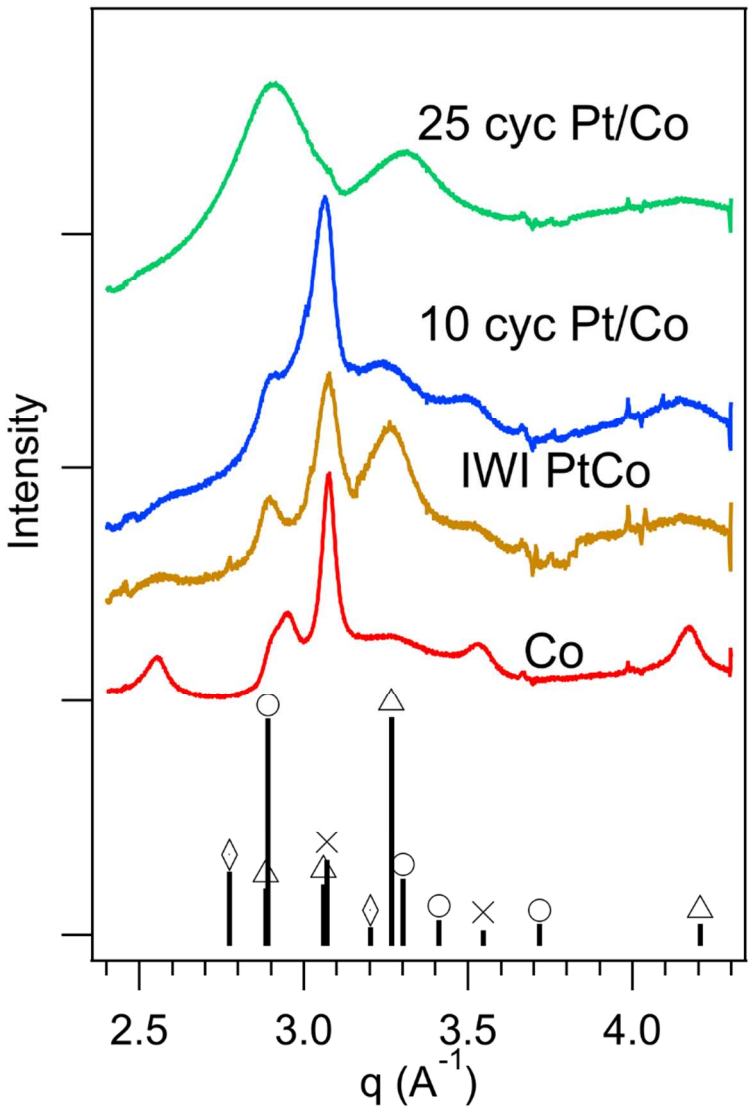

Figure 3. Powder x-ray diffraction of catalysts after reduction. The 25 cyc $Pt/Co/SiO_2$ catalyst shows bulk alloying in a PtCo phase. The other catalysts show HCP and FCC Co phases. Lines at bottom are FCC Co (crosses), HCP Co (triangles), PtCo (circles), and Pt (diamonds) (PDF cards 00-015-0806, 01-071-4652, and 01-071-7406, 00-004-0802, respectively).

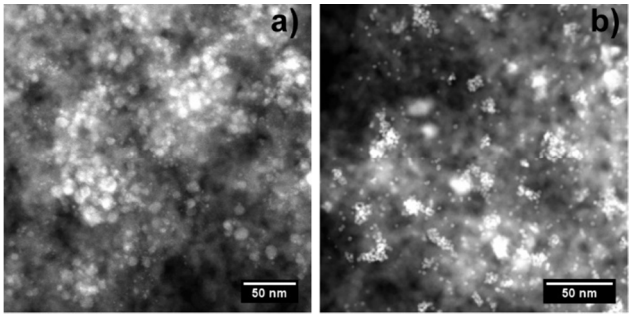

Figure 4. Dark field STEM images collected after reduction of a) IWI $PtCo/SiO_2$ b) 25 cyc $Pt/Co/SiO_2$. Scale bars are 50 nm.

CO uptake measurements, which allow for comparisons of the number of active sites on the catalysts, were performed on the post-reduction catalyst samples. A typical CO chemisorption measurement is presented in the Supporting Information (Figure S2), and the CO uptake results are summarized in Table 1. Calculated metal surface areas based on the CO chemisorption measurements are provided in the Supporting Information (Table S1). The chemisorption measurements show that there is an increase in CO uptake with increasing ALD Pt loading, from 28 μmol CO/g catalyst for the unmodified Co/SiO_2 to 68 μmol CO/g for Co with the highest ALD Pt loading. This increase can be primarily explained by CO chemisorption directly on Pt nanoparticles deposited by ALD, as evident by the CO uptake values for SiO_2 samples containing only Pt, also shown in Table 1. In the case of the cobalt catalyst with 10 cycles of Pt ALD, the total uptake (55 μmol/g) corresponds well to the sum of the ALD Pt/SiO_2 catalyst (23 μmol/g) and Co/SiO_2 catalyst (28 μmol/g) uptakes, indicating there is not a significant change in Co dispersion after the addition of ALD Pt. For the case of the 25 cyc $Pt/Co/SiO_2$ catalysts, however, the uptake is lower than expected from the linear combination. This can be explained by the formation of an alloy in the catalyst which would result in a reduction in the number of separate Pt nanoparticles and thus the CO uptake. Another potential explanation is that at these

numbers of ALD Pt cycles, there is a very high coverage of Pt on the SiO_2 surface and thus the Pt nanoparticles are packed much more closely together which may encourage sintering effects.

The IWI $PtCo/SiO_2$ catalyst has a lower CO uptake than the other catalysts. Prior work has shown that pH can play a significant role in the wetness impregnation process, and the addition of the acidic H_2PtCl_6 precursor may affect the overall cobalt dispersion, affecting its surface area.[32] Poisoning by chlorine is another potential explanation for the lower CO uptake for this sample. However, we consider this option unlikely since the activity of the IWI $PtCo/SiO_2$ catalyst prepared using H_2PtCl_6 is similar to that of the other prepared Co-based catalysts for which there is no expected source of chlorine impurities (Table 2). Moreover, XPS analysis shows that reduction successfully removes chlorine from the IWI $PtCo/SiO_2$ catalyst and that the other catalysts do not contain any detectable chlorine levels (Figure S3). Surface areas and pore size distributions for selected catalysts are provided in Figure S4.

Table 1: Catalyst CO uptake values measured using chemisorption

Catalyst	**CO uptake (μmol CO /g catalyst)**
Co/SiO_2	28
IWI $PtCo/SiO_2$	19
5 cyc $Pt/Co/SiO_2$	39
10 cyc $Pt/Co/SiO_2$	55
25 cyc $Pt/Co/SiO_2$	68
10 cyc Pt/SiO_2	23
25 cyc Pt/SiO_2	70

Reaction testing selectivity and activity results are presented in Table 2. All Co-containing catalysts were tested under similar conversion conditions (1-3% based upon detected products)

with a cobalt metal loading of ~10 wt%. Controls of ALD Pt/SiO_2 catalysts were tested at <0.1% conversion due to their very low activities. Testing at low conversion conditions is selected because it minimizes the effects of secondary reactions[33] and ensures the reaction is not diffusion limited.[34] Catalyst stoichiometries were determined using ICP and the mass ratios of Pt to Co are also provided in Table 2. As seen in Table 2, the activities, measured as μmol CO/g catalyst*s, were significantly lower for the pure Pt catalyst samples (10 cyc Pt and 25 cyc Pt) compared with the Co-containing catalysts. Reaction testing of cobalt on SiO_2 catalysts shows that the primary products are hydrocarbons with some modest selectivity toward methanol and higher alcohols. Overall, a reduction in activity is observed after the addition of Pt by ALD. This decrease could result from blocking of surfaces sites by Pt. With increasing ALD cycles, and thus increasing Pt loading and Pt nanoparticle size, there is also increasing selectivity towards methanol and reduced selectivity towards longer chain hydrocarbons (C_5-C_9). With the addition of Pt using 10 and 25 cycles of Pt ALD, there is a moderate increase in higher alcohol selectivity. These effects are not pronounced at lower Pt loadings in the case of 1 and 5 Pt ALD cycles. The catalyst prepared using incipient wetness impregnation of Pt and Co salts has similar selectivity to the 5 cyc Pt/Co catalysts which has the closest Pt weight loading of the ALD prepared samples. The results with increasing Pt content for the catalysts prepared by ALD are consistent with literature reports on the effect of Pt on Co catalysts. Work by Eschemann et al. also showed that Pt promotion of Co catalysts on titania reduced selectivity towards longer chain hydrocarbon products.[10] Other studies have shown a trend in which there is a transition from hydrocarbon selectivity towards methanol as the primary product at higher Pt loadings.[4,11] We note that although the 10 cyc Pt/SiO_2 and 25 cyc Pt/SiO_2 catalysts have selectivity towards methanol and methane, the activity of Pt alone is very low and hence the combination of uninteracting Pt and

Co sites cannot on its own explain the changes in selectivity. The activity and selectivity of the prepared catalysts for methanol are much lower than those of Cu/ZnO methanol synthesis catalysts;[35,36] however, Cu/ZnO catalysts have reduced performance in CO H_2 mixtures without CO_2.[37]

Table 2: CO hydrogenation reaction testing. Carbon-weighted selectivities and activities for different catalysts. The mass ratio determined using ICP elemental analysis is given as Pt/Co. Replicate testing was performed for the Co and 25 cyc Pt/Co catalysts and the corresponding averages and standard deviations are reported.

		Selectivity (%)					**Activity (µmol CO/g catalyst*s)**
Catalyst	**Pt/Co**	**MeOH**	**C_{2+} OH**	**CH_4**	**C_2-C_4 HC**	**C_5-C_9 HC**	
Co/SiO_2		0.6±0.2 %	1±0.6%	24±4 %	23±1%	51±5%	8
1 cyc $Pt/Co/SiO_2$	0.004	2%	1%	25%	21%	52%	4
5 cyc $Pt/Co/SiO_2$	0.13	2%	1%	26%	25%	46%	11
10 cyc $Pt/Co/SiO_2$	0.20	3%	2%	32%	29%	34%	4
25 cyc $Pt/Co/SiO_2$	0.80	16±2%	3±0.1%	35±2 %	22±1%	24±3%	4
10 cyc Pt/SiO_2		52%	0%	48%	0%	0%	0.01
25 cyc Pt/SiO_2		86%	0%	13%	1%	0%	0.2
IWI $PtCo/SiO_2$	0.15	2%	2%	25%	26%	45%	11

To understand how the surface chemistry at the cobalt catalyst is affected by the addition of platinum, we performed real time, *in situ* DRIFTS measurements. Prior work has demonstrated

that *in situ* spectroscopic measurements are crucial in understanding a catalyst's surface chemistry and reaction intermediates.[38] Using *in situ* DRIFTS, we can monitor the evolution of surface species as a CO-saturated catalytic surface is hydrogenated and identify CO binding sites. The results for various catalyst samples are shown in Figures 5 – 9.

To complement the IR measurements, DFT calculations were performed to determine the correlations between the different CO binding configurations and their vibrational frequencies (Figure 10). Calculations were performed for the stepped 211 and the close-packed 111 surfaces of pure Co, Pt and Pt-Co alloys of varying compositions (adsorption energies and CO vibrational frequencies for all systems studied are tabulated in the Supporting Information, Table S1). The alloy configurations were constructed based on the Pt_3Co and Co_3Pt stoichiometries of the bulk FCC metal. Selected calculated CO binding energies on stepped 211 surfaces are presented in Table 3. On stepped 211 surfaces, the CO binding energy decreases as the stoichiometry varies from pure Co to pure Pt (Table 3). Figure 10 presents the vibrational frequency of CO as a function of the surface Pt:Co ratio for on-top (also called "linear"), bridging, and three-fold CO binding configurations. We find that the vibrational frequencies are most strongly correlated with the binding configuration rather than the binding strength of CO, as the vibrational modes clearly separate into on-top, bridging, and three-fold binding configurations (Figure 10, Figure S5, Table S2). As Pt alloys become more Co rich there is a slight red shift in CO vibrational frequencies on Pt sites in agreement with the d band model: Pt-Co surfaces shifting up towards the Co d-band center from the lower Pt d-band center results in increased electron donation to the CO π^* orbital.[39] The only weak dependence on factors beyond the CO configuration suggests that the vibrational frequency is a robust measure of the adsorption configuration. By comparing

calculated to experimental IR absorption spectra, the type of binding configuration can be assigned.

In the DRIFTS spectra of CO on the Co/SiO_2 catalyst (Figure 5) before hydrogenation (t=0), there is a strong absorbance peak with components at 2068 cm^{-1} and 2043 cm^{-1}, together with weaker peaks at 2185 cm^{-1} and ~1810 cm^{-1}. The peak at 2043 cm^{-1} results from linearly adsorbed CO.[40,41] Based upon prior work on Co supported on SiO_2, the 2068 cm^{-1} peak is assigned to CO adsorbed on partially oxidized Co species.[25,41] The weak peak at 2185 cm^{-1} is in the range ascribed to CO adsorbed on oxidized Co^{2+} and Co^{3+} species.[42–45] This peak can be attributed to residual oxidized Co species due to the difficulty in fully reducing an unpromoted Co catalyst. The weak broad feature circa 1810 cm^{-1} corresponds to CO at Co three-fold hollow sites.[46] During hydrogenation (t=1 through t=16 min), there is a rapid transition of the principal (linear CO) peak into a lower frequency peak at 1957 cm^{-1} that is in the ~1900-2000 cm^{-1} range typically assigned to bridging CO on Co.[3,40,46,47] Changes in coverage alone do not explain this frequency shift, because spectra collected when CO is simply allowed to desorb do not show such a shift (Figure S6). Hence, the shift seen in Figure 5 suggests a transition from linear CO to bridging CO in the presence of H_2. Prior work on CoRe observed a similar transition during hydrogenation.[25] The observed CO bridging vibrational frequencies on Co are at higher frequencies than those obtained by the DFT calculations. Although there is not quantitative agreement between the predicted vibrational frequencies and the experimental values, we observe the same ordering in terms of CO binding configurations. The shift may be explained by uncertainty in the absolute values of the DFT calculations and the low coverage of CO used in the calculations. Control measurements were performed under vacuum without the addition of H_2 (Figure S6). In these measurements, the changes in peak position observed during H_2

exposure (Figure 5) were not observed without H_2 (Figure S6). In addition, a much low rate of attenuation in absorbance was observed (Figure S6). Based on these differences, we conclude that the changes during *in situ* DRIFTS measurements under H_2 can be attributed to hydrogenation and not simple desorption or displacement reactions. This methodology has been successfully demonstrated in several prior studies.[25,48,49] Further, Co is an active CO hydrogenation catalyst at the temperatures used for the DRIFTS (250 °C).

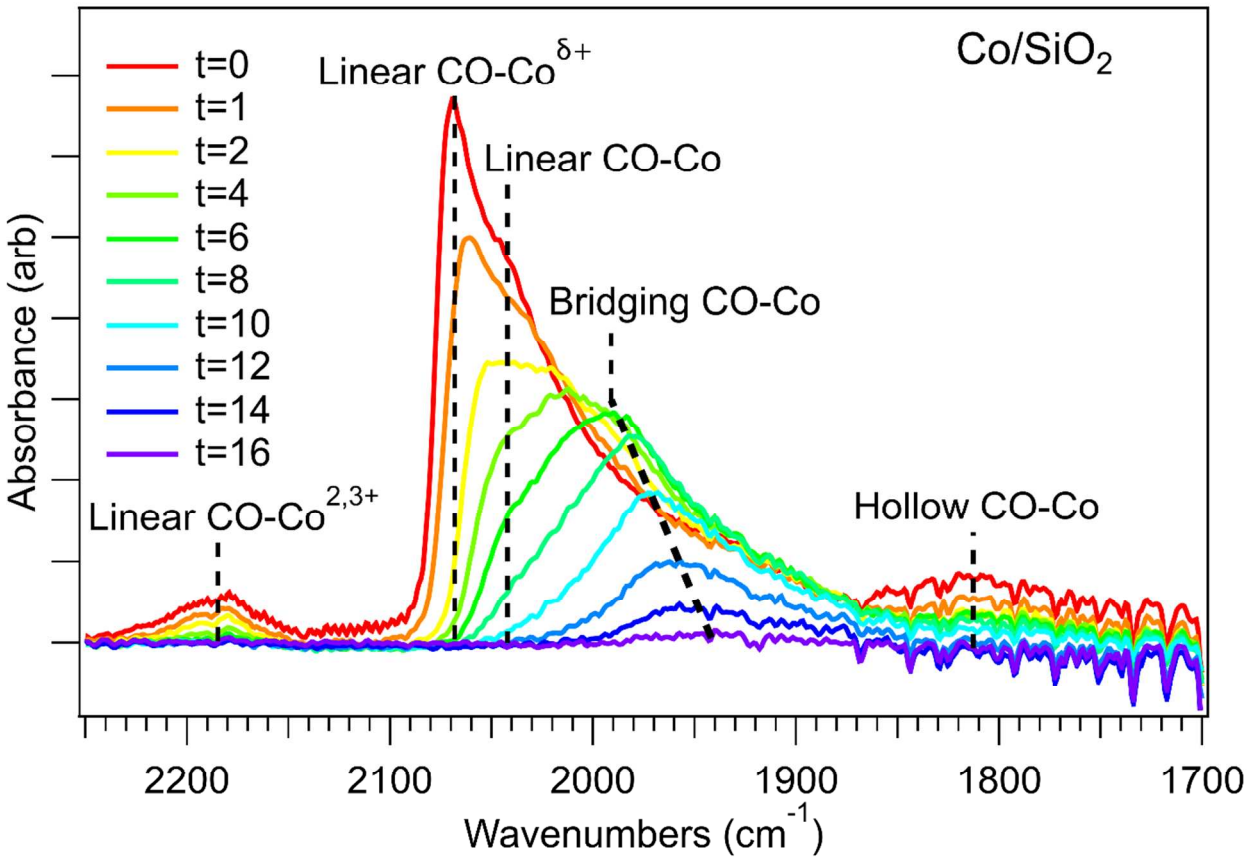

Figure 5. A series of DRIFTS spectra collected in a time series during hydrogenation of CO on a Co/SiO_2 catalyst at 250 ^{o}C. In the presence of hydrogen, the linear cobalt-CO peak converts to a bridging peak that is subsequently hydrogenated. Time is given in minutes.

For the sample for which Pt is deposited using 10 cycles of Pt ALD on SiO_2, two peaks are observed in the DRIFTS spectrum initially (t=0) at 2064 cm^{-1} and 2084 cm^{-1} (Figure 6). Single crystal studies of CO adsorbed on Pt 111 have shown IR absorptions at 2084 cm^{-1} and 1850 cm^{-1}, corresponding to CO bonded at linear and bridging sites, respectively.[50] The two peaks seen in Figure 6 can be attributed to CO bound linearly to Pt on sites with different coordination numbers.[51] Due to increased d electron density at undercoordinated sites, there is high π^* backbonding from the metal d orbital to the CO π^* system, resulting in a decreased CO vibrational frequency. The peak at 2084 cm^{-1} is blue-shifted and corresponds to Pt sites with higher coordination, such as terraces, in agreement with prior reports.[52,53] The red-shifted peak corresponds to Pt atoms in a lower coordination environment and can be attributed to edges, kinks, or other low-coordination Pt surface sites and agrees with the ranges measured in prior nanoparticle and single crystal studies.[51,52] The relative frequencies of CO bonded to high- and low-coordinated Pt sites are also confirmed by the DFT calculations provided in Table S1, in which CO linearly bound to Pt(111) has a vibrational frequency about 20 cm^{-1} higher than that bound to Pt(211). No CO bridging peak on Pt, expected at ~1800 cm^{-1}, is observed on the prepared 10 cyc Pt/SiO_2 catalyst; however, this peak tends to be weak in intensity and difficult to observe.[54] The bridging peak may also be absent due to particle size effects or due to the weak nature of the absorption.[54] Upon hydrogenation (t=2 through t=118 min), both linear CO peaks decay slowly with time which agrees with the strong binding of CO by platinum. During hydrogenation, the peaks also red shift. The shifts can be explained by the lower CO coverages as hydrogenation proceeds: at lower coverage there is more effective Pt d electron density per CO, thus greater backdonation to the CO π^* system, and hence a weakening of the CO bond which is reflected in the lower vibrational frequency.[55] The same slight redshift is observed upon

desorption in the absence of H_2 (Figure S7). Therefore, in contrast to the CO/Co system, on Pt the change occurring with hydrogenation can be attributed strictly to coverage effects.

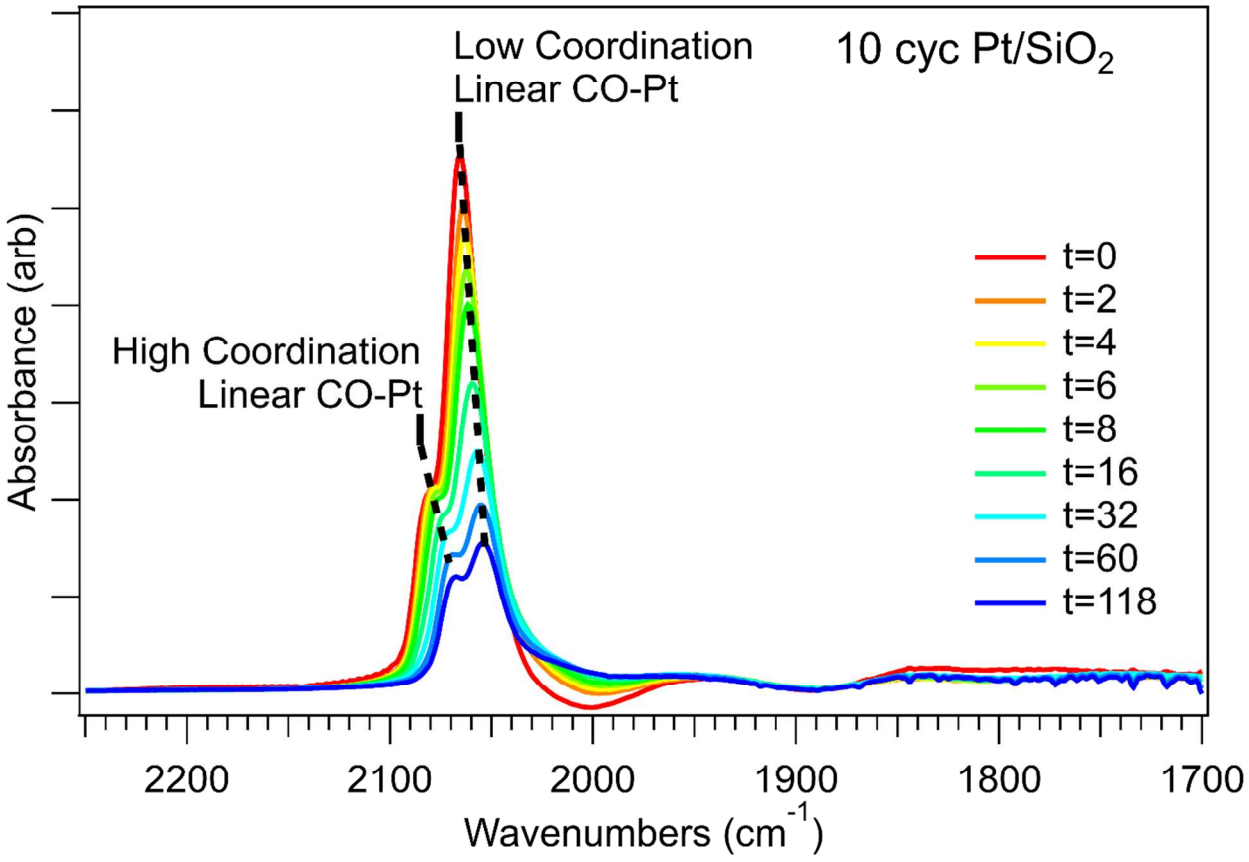

Figure 6. A series of DRIFTS spectra collected in a time series during hydrogenation of CO on a 10 cyc Pt/SiO_2 catalyst at 250 ^oC. Two linear peaks are present corresponding to platinum sites with different coordination numbers. Time is given in minutes.

The Pt-Co catalyst promoted using ALD (10 cyc $Pt/Co/SiO_2$) shows behavior resulting from the presence of both Pt and Co. For these samples, DRIFTS spectra monitored during hydrogenation (Figure 7), show that there are peaks present at t=0 near 1810 cm^{-1}, 1990 cm^{-1}, 2044 cm^{-1}, 2061 cm^{-1}, and 2079 cm^{-1}.

The peaks at 2079 cm^{-1} and 2061 cm^{-1} correspond closely to those observed for 10 cyc Pt/SiO_2 samples and are assigned to linear CO at high coordination and low coordination Pt sites,

respectively. Prior work has shown a correlation between the CO vibrational frequency and Pt nanoparticle size.[51,52] The presence of CO-Pt peaks at similar frequencies on the 10 cyc Pt/SiO_2 catalyst and the 10 cyc Pt/Co/silica catalyst indicates there are still Pt nanoparticles present of similar sizes on the two catalysts after reduction. The peaks on 10 cyc $Pt/Co/SiO_2$ catalyst are mildly red-shifted compared with the 10 cyc Pt/SiO_2 catalyst; however, this shift is not significant relative to the coverage-dependent frequency shifts. Several groups have noted that with the addition of metallic cobalt, the linear CO-Pt vibrational frequency decreases.[39,50,56,57] We note a similar trend in our performed DFT calculations (Figure 10). Because there is little shift on the CO stretching frequency from the case of Co/SiO_2 and because our DFT calculations (Figure 10) demonstrate that the linear stretching frequency is a highly sensitive probe of the binding site, we assign the peak at 2044 cm^{-1} to linear CO bonded to a Co-based site. The component near 1957 cm^{-1} corresponds to the range typically reported for bridging CO on Co and is therefore assigned as such.[3,40,46,47] Similar to the case of Co/SiO_2, a peak due to CO at three-fold hollow Co sites is observed near 1810 cm^{-1}.

During hydrogenation of the 10 cyc $Pt/Co/SiO_2$ catalyst, the 2044 cm^{-1} linear CO-Co vibrational peak attenuates while a bridging CO-Co peak grows in, similar to the case of the Co/SiO_2 catalyst. Unlike the Co/SiO_2 catalysts, however, the 10 cyc $Pt/Co/SiO_2$ catalyst retains some linearly bound CO-Co during the hydrogenation process. Concurrently, the peaks associated with the Pt in the ALD $Pt/Co/SiO_2$ catalyst undergo a decay and redshift as they did for the pure 10 cyc Pt/SiO_2 sample; however, the decay is much more rapid in the mixed catalyst case. This result indicates that the CO present on the Pt species is being hydrogenated much more rapidly when interacting with Co compared with Pt supported on SiO_2 with no cobalt present. DRIFTS spectra acquired in a 2:1 H_2:CO ratio are included in Figure S10. Note that the

data in Figure S10 are expected to differ from those in Figures 5-9 because in the former, the measurements provide steady state information on surface species present under CO/H_2 conditions, whereas in the latter, the measurements provide information about CO reactivity and transient species. We find that during steady state CO/H_2 exposure, CO binds in configurations similar to those observed in the presence CO without H_2. The minor change in peak ratios may result from competitive adsorption of H_2.

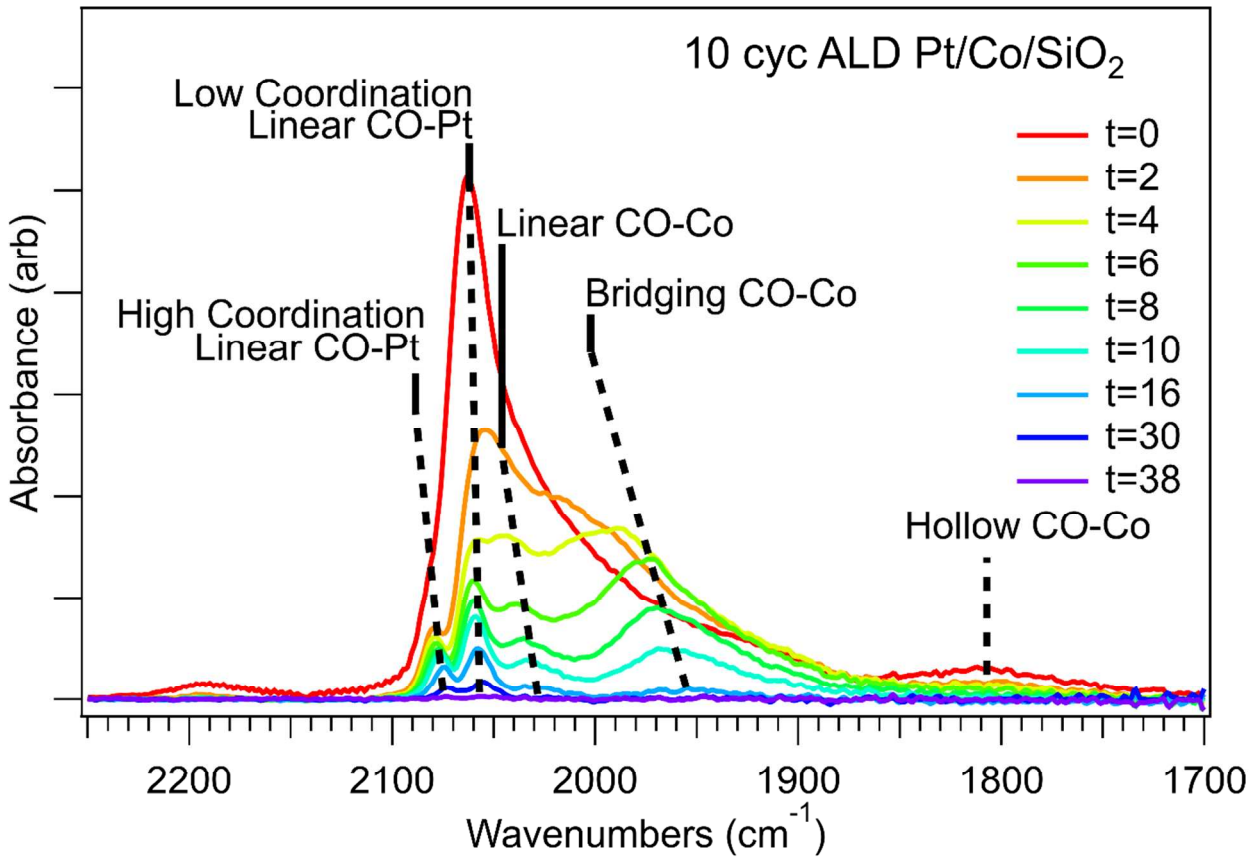

Figure 7. A series of DRIFTS spectra collected in a time series during hydrogenation of CO on a 10 cyc $Pt/Co/SiO_2$ catalyst at 250 ^{o}C. Linear CO peaks corresponding to Pt sites are present. Linear and bridging CO peaks corresponding to cobalt-based sites are also present.

The Pt-Co catalyst promoted using additional ALD cycles (25 cyc Pt/Co/SiO_2) again shows behavior resulting from the presence of both Pt and Co. For these samples, DRIFTS spectra acquired during hydrogenation (Figure 8), show that there are peaks present at t=0 near 1785 cm^{-1}, 2010 cm^{-1}, 2058 cm^{-1}, and 2075 cm^{-1}. The CO-Pt feature (2075 cm^{-1}) due to high coordination Pt sites is observed and no peaks due to low coordination CO-Pt sites are observed in contrast to the 10 cyc Pt/Co/SiO_2 catalyst. This difference is attributed to the larger Pt particles on the 25 cyc Pt/Co/SiO_2 catalyst having a lower fraction of undercoordinated surface Pt sites. The peak at 2058 cm^{-1} is assigned as linear CO bonded to a Co-based site and the peak at 2010 cm^{-1} to bridging CO bonded to a Co site as discussed for the 10 cyc Pt/Co/SiO_2 catalyst. The increased frequency of these sites can be explained by more Pt-Co interactions on this sample as there is an increased Pt loading. The intensity of the CO-Pt feature is much more intense than the Co features due to the high amount of Pt deposited compared with the 10 cyc Pt/Co/SiO_2 catalyst (Figure 7). As discussed above, a peak due to CO-Co at threefold sites is observed near 1785 cm^{-1}.

During hydrogenation of the 25 cyc Pt/Co/SiO_2 catalyst, the CO-Co peaks decrease in intensity. Relative to the 10 cyc Pt/Co/SiO_2 catalyst, the 25 cyc Pt/Co/SiO_2 catalyst has a greater fraction of linear CO-Co to bridging CO-Co. The linear CO-Pt peak attenuates in intensity; however, it does so at a much slower rate than for the more lightly Pt-promoted Co/SiO_2. We expect this behavior as this catalyst contains a high concentration of Pt, leading to more Pt sites that are not interacting with Co (Figure 4) and slowly hydrogenate CO (Figure 6).

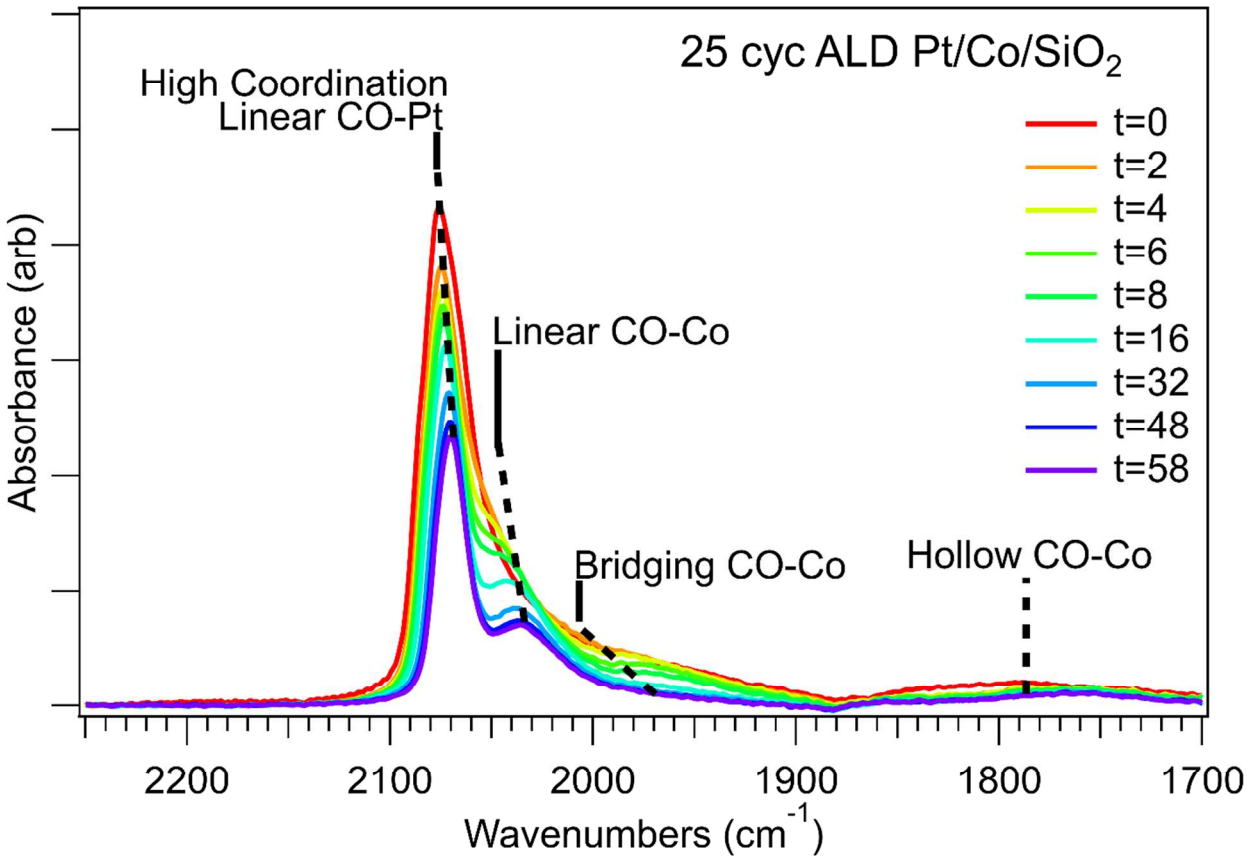

Figure 8. A series of DRIFTS spectra collected in a time series during hydrogenation of CO on a 25 cyc $Pt/Co/SiO_2$ catalyst at 250 ^oC. A peak corresponding to linear CO-Pt at high coordination Pt sites is observed. Linear and bridging CO peaks corresponding to cobalt-based sites are also present. Time is given in minutes.

In the case of the IWI $PtCo/SiO_2$ catalyst, three peaks are present (appearing at c. 2000 cm^{-1}, 2052 cm^{-1}, and 2063 cm^{-1} at t=0 min) in the DRIFTS spectra during hydrogenation (Figure 9). Based on the above discussion, we assign the peaks at 2052 cm^{-1} and 2063 cm^{-1} to CO linearly bonded to PtCo sites. We assign the peak near 2000 cm^{-1} to bridging CO on PtCo alloy sites based on the assigned spectra of CO on Co/SiO_2 (Figure 5). The XRD measurements performed on this catalyst (Figure 3) did not support the presence of a bulk alloy; however, surface sensitive

measurements using DRIFTS are consistent with the formation of an alloy. The combination of these two results indicates that the alloying is primarily at the surface and not in the bulk. Although there are stable bulk alloys of Pt and Co, prior work has noted the preference for surface segregation.[58,59] Given the stronger binding of CO by Pt than Co (Table 3), we expect the segregation effects to be enhanced in the presence of syngas. During hydrogenation, the peaks red-shift. We attribute this change to reduction in CO coverage based upon the discussion above. Similar to the 10 cyc $Pt/Co/SiO_2$ catalyst, the IWI $PtCo/SiO_2$ catalyst has substantial bridging and linear CO species present throughout the hydrogenation of adsorbed CO.

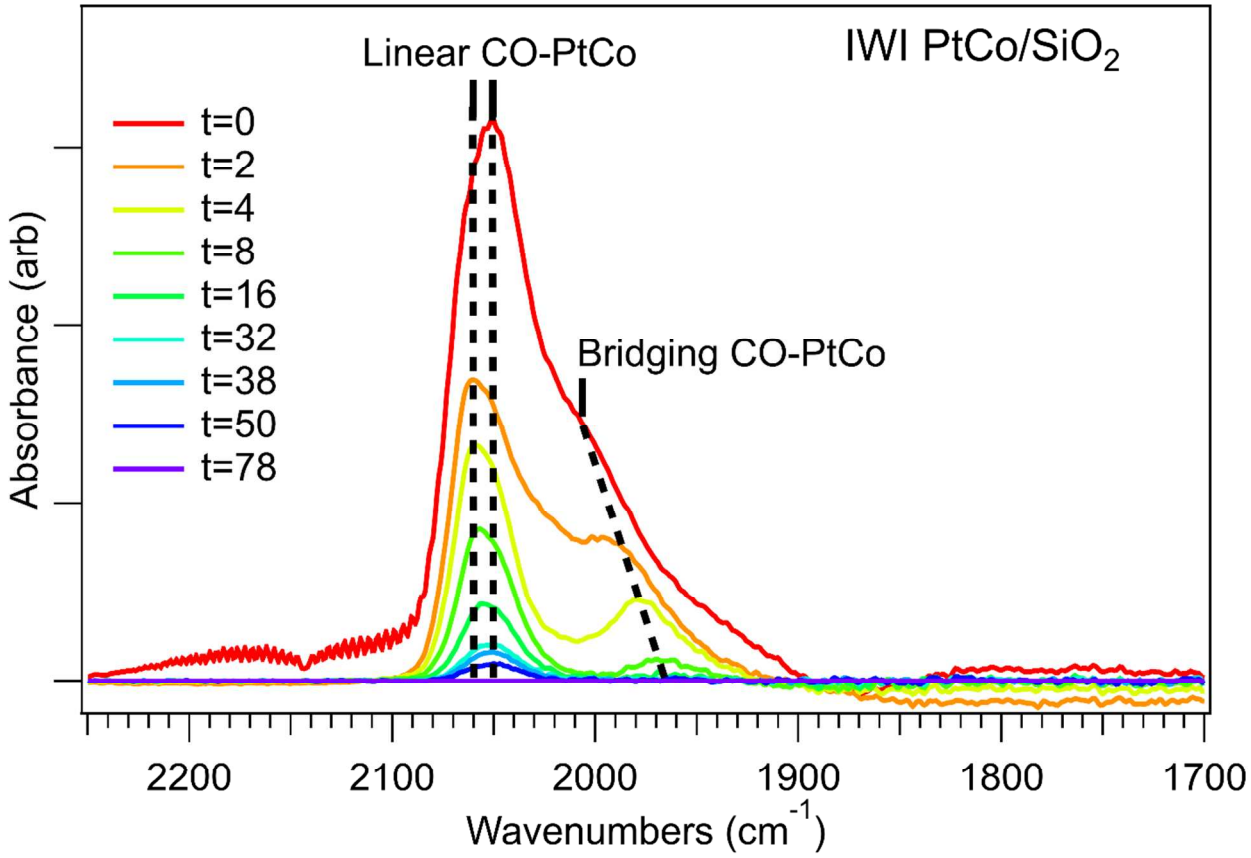

Figure 9. A series of DRIFTS spectra collected in a time series during hydrogenation of CO on a IWI $PtCo/SiO_2$ catalyst at 250 ^{o}C. Peaks corresponding to linear and bridging CO are observed that are both assigned to a PtCo alloy phase. Time is given in minutes.

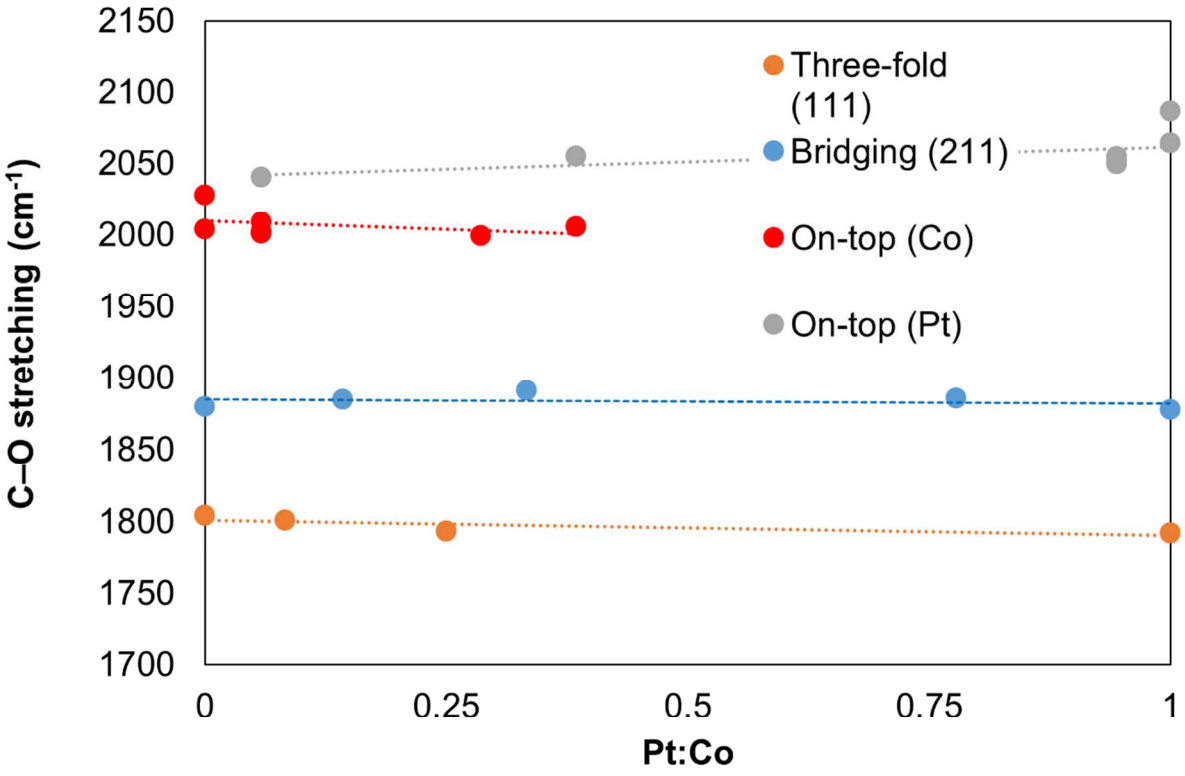

Figure 10. Calculated CO vibrational frequencies as a function of Pt:Co ratio on different Pt, Co, and Pt-Co surface configurations. The points are color coded by the binding configuration and the metal of the binding site, with CO bound in a linear configuration to Pt in gray, CO bound in a linear configuration to Co in red, CO bound in a bridging configuration on 211 surfaces in blue, and CO bound in a three-fold configuration on 111 surfaces in orange. The vibrational frequencies cluster into different frequency ranges based upon the binding configuration. Representative images of CO bound in linear, bridging, and three-fold configurations are shown with Pt atoms in gray and Co in red.

Table 3: DFT-Calculated Binding Energies of Linear CO on Selected 211 Surfaces

Surface	**CO binding energy (eV)**
Pt	-1.79
Pt_3Co	-1.69
Pt Overlayer	-1.62
Co_3Pt	-1.61
Co	-1.52

Discussion:

In CO hydrogenation, there are several kinetically competing pathways leading to the production of methanol, higher alcohols, hydrocarbons and other oxygenate products. In examining these processes, the cleavage of the C-O bond, or lack thereof, plays a crucial role in formation of the final products. For hydrocarbons in Fischer-Tropsch synthesis, the precise mechanism is debated in the literature, with dominant proposals being the carbide mechanism and CO insertion.[1] CO insertion is the most commonly accepted mechanism for higher alcohol formation;[3,5,41,60–62] however, there are other proposals.[63] In the CO insertion mechanism, CO bond cleavage and hydrogenation form CH_x fragments, and these fragments then undergo a CO insertion, or coupling, event in which an adsorbed CO molecule inserts into a metal—CH_x bond. In the case where the CO bond dissociates after insertion, hydrocarbons would be formed; if the bond does not dissociate, higher alcohols and other oxygenates would result. In the carbide

mechanism, CO dissociates to form CH_x fragments on the surface which subsequently undergo C-C coupling to form hydrocarbons.[1,63] In both mechanisms, when there is high CO dissociation, methane and hydrocarbons are expected as the primary products. In the case where the CO bond doesn't dissociate, methanol would be expected as a major product.

With the addition of Pt, we observed notable changes in hydrogenation behavior monitored using DRIFTS that, together with the results of our DFT calculations, support the conclusion that changes are occurring to the active site. In the DRIFTS of Co/SiO_2 during hydrogenation, there is primarily bridging CO present. Bridging CO on Co is generally agreed to be the active species in Fischer-Tropsch synthesis of alkanes,[25,64,65] in which CO dissociates to form hydrocarbons. With increasing Pt content (0, 10, 25 cycles ALD Pt), however, the DRIFTS results show that there is an increase in linearly adsorbed CO relative to bridging CO during hydrogenation. Prior work has shown CO in a linear configuration is less prone to dissociate.[25,64,65] An increase in CO dissociation would result in increased surface CH_x species, and these CH_x species can form growing hydrocarbon chains through C-C coupling steps.[1] On the other hand, with a decrease in CO dissociation there would be a decrease in surface CH_x species. This reduction in surface alkyl fragments would reduce the chain growth probability and thus favor the production of short chain hydrocarbons. We observed with increasing Pt content that the hydrocarbon distribution shifts from primarily C_5-C_9 to C_1-C_5 hydrocarbons, consistent with a decrease in CO dissociation.

On the $Pt\text{-}Co/SiO_2$ catalysts prepared using Pt ALD, in addition to shifting selectivity towards short chain hydrocarbons, there is a substantial increase in methanol selectivity. We propose two possible explanations for this behavior. Looking at the peaks from CO on Pt in DRIFTS, the linear Pt-CO absorbances decay much more rapidly on the Pt sites of the 10 cyc $Pt/Co/SiO_2$ catalyst compared with the 10 cyc Pt/SiO_2 catalyst during hydrogenation. This change indicates

that CO bound to the Pt "supported" on Co has a much higher hydrogenation rate. Prior work has shown that the addition of transition metals, such as Fe, can reduce binding energy of CO on Pt.[66] In agreement, our DFT calculations show CO binds more weakly on Co compared to Pt 211, and the alloyed Pt-Co 211 surfaces considered herein have an intermediate binding strength (Table 3). CO strongly binds to Pt and readily poisons Pt surfaces in the presence of H_2.[67] The increased rate of hydrogenation during *in situ* DRIFTS measurements and the reduction in binding energy on Pt-Co versus Pt point to a reduction in the barrier for CO hydrogenation on Pt-Co versus Pt. Therefore, we propose that the Pt sites interacting with Co have an overall higher activity toward methanol production. A second possibility is that changes in a Co-based site could give rise to the increased methanol selectivity. The reduced chain growth after the addition of Pt could indicate a reduction in CO dissociation. This reduction in CO dissociation would favor methanol production. We note that full microkinetic modelling beyond the scope of this study would be required to verify these proposals.

Prior work has noted that as chain growth probability increases, oxygenate selectivity decreases.[1] Consistent with this idea, the addition of Pt to Co both reduces the hydrocarbon chain growth and increases the methanol selectivity. Pt likewise increases the selectivity of the prepared Co/SiO_2 catalysts towards higher alcohols. Higher alcohol formation requires a balance between surface CO dissociation and insertion. Consistent with this picture, studies on Co-based catalysts have proposed an important balance between dissociated and nondissociated CO for higher alcohol synthesis.[41,60,68,69] Work on mixed Co and Co_2C catalysts has also shown the importance of having both dissociatively and non-dissociatively bound CO in obtaining higher selectivity to ethanol.[68] For CuCo catalysts, the selectivity has also been reported to be a balancing act between dissociated and nondissociated CO.[41,60] The addition of Cu blocks Co sites

for CO dissociation and provides nondissociated CO species for CO insertion.[60] All of these results support the idea that on a Fischer-Tropsch catalyst such as cobalt, in which CO dissociation is relatively facile, a decrease in CO dissociation would decrease surface CH_x species and disfavor the polymerization reaction that results in the formation of alkanes through Fischer-Tropsch catalysis. Hence, the interplay between dissociated and nondissociated CO is a critical factor in achieving selectivity towards higher alcohols with the addition of a second species to Co allowing for an increase in nondissociated CO. Consistent with this discussion, shifting the balance between dissociated and nondissociated CO leads to improved selectivity towards higher alcohols. Taken all together, we observed that the addition of Pt increases linearly-bound CO species, resulting in less CO dissociation and a shift in the selectivity towards more higher alcohols and methanol, and fewer long chain hydrocarbons.

Conclusions:

The selectivity of Pt-promoted Co/SiO_2 catalysts toward alcohol synthesis was investigated using catalysts prepared by ALD and IWI syntheses with the use of ALD allowing for the systematic variation of Pt content in a highly controlled manner. The catalysts were characterized using a variety of *ex situ* techniques and *in situ* DRIFTS experiments, complemented by DFT calculations. The addition of Pt resulted in increased selectivity towards methanol and higher alcohols, and reduced selectivity towards long chain hydrocarbons. Through *in situ* DRIFTS measurements, we found that the addition of Pt increases linearly bound surface CO which in turn we attribute to reduced CO dissociation, increased methanol and higher alcohol selectivity, and reduced long chain hydrocarbon selectivity. Although the performance of these catalysts is not expected to compete with industrial Cu-based methanol synthesis catalysts, this system

represents an interesting model case for mechanistic studies. We demonstrated experimentally for the first time using *in situ* DRIFTS the role of different CO binding sites in CO hydrogenation on Pt-Co. This work confirms the trends noted in CO hydrogenation between the roles of sites for nondissociated CO binding and CO dissociation. We also showed the strength of ALD as a means for promoting catalysts. The methods used in this study can be applied to study the promotion of bimetallic catalytic systems in a robust and reproducible manner. Although ALD has yet to be applied for commercial catalysts, current technology allows for industrial scale production of ALD-coated powders.

ASSOCIATED CONTENT

Supporting Information.

The following files are available free of charge.

Temperature-programmed reduction, XPS characterization, BET characterization, DRIFTS desorption measurements, and chemisorption supporting information.pdf

AUTHOR INFORMATION

Corresponding Author

*sbent@stanford.edu

Author Contributions

The manuscript was written through contributions of all authors. All authors have given approval to the final version of the manuscript.

ACKNOWLEDGMENT

We acknowledge financial support from the U.S. Department of Energy, Office of Basic Energy Sciences to the SUNCAT Center for Interface Science and Catalysis. This material is based upon work supported by the National Science Foundation Graduate Research Fellowship under Grant No. DGE-114747. Use of the Stanford Synchrotron Radiation Lightsource, SLAC National Accelerator Laboratory, is supported by the U.S. Department of Energy, Office of Science, Office of Basic Energy Sciences under Contract No. DE-AC02-76SF00515. The authors gratefully acknowledge the use of the Stanford Nano Shared Facilities (SNSF) of Stanford University for sample characterization. The authors would like to thank Andrew Riscoe for performing the BET measurements

REFERENCES

(1) van Santen, R. A.; Markvoort, A. J.; Filot, I. A. W.; Ghouri, M. M.; Hensen, E. J. M. Mechanism and Microkinetics of the Fischer-Tropsch Reaction. *Phys. Chem. Chem. Phys.* **2013**, *15*, 17038–17063.

(2) Matsuzaki, T.; Takeuchi, K.; Hanaoka, T. Effect of Transition Metals on Oxygenates Formation from Syngas over Co / SiO ,. **1993**, *105*, 159–184.

(3) Matsuzaki, T.; Hanaoka, T.; Takeuchi, K.; Arakawa, H.; Sugi, Y.; Wei, K.; Dong, T.; Reinikainen, M. Oxygenates from Syngas over Highly Dispersed Cobalt Catalysts. *Catal. Today* **1997**, *36*, 311–324.

(4) Christensen, J. M.; Medford, A. J.; Studt, F.; Jensen, A. D. High Pressure CO

Hydrogenation Over Bimetallic Pt–Co Catalysts. *Catal. Letters* **2014**, *144*, 777–782.

(5) Medford, A. J.; Lausche, A. C.; Abild-Pedersen, F.; Temel, B.; Schjødt, N. C.; Nørskov, J. K.; Studt, F. Activity and Selectivity Trends in Synthesis Gas Conversion to Higher Alcohols. *Top. Catal.* **2014**, *57*, 135–142.

(6) Cao, R.; Pan, W. X.; Griffin, G. L. Direct Synthesis of Higher Alcohols Using Bimetallic Copper/cobalt Catalysts. *Langmuir* **1988**, *4*, 1108–1112.

(7) Subramanian, N. D.; Balaji, G.; Kumar, C. S. S. R.; Spivey, J. J. Development of Cobalt-Copper Nanoparticles as Catalysts for Higher Alcohol Synthesis from Syngas. *Catal. Today* **2009**, *147*, 100–106.

(8) Xiang, Y.; Chitry, V.; Liddicoat, P.; Felfer, P.; Cairney, J.; Ringer, S.; Kruse, N. Long-Chain Terminal Alcohols through Catalytic CO Hydrogenation. *J. Am. Chem. Soc.* **2013**, *135*, 7114–7117.

(9) Xiang, Y.; Kruse, N. Tuning the Catalytic CO Hydrogenation to Straight- and Long-Chain Aldehydes/alcohols and Olefins/paraffins. *Nat. Commun.* **2016**, *7*, 13058.

(10) Eschemann, T. O.; Oenema, J.; de Jong, K. P. Effects of Noble Metal Promotion for Co/TiO2 Fischer-Tropsch Catalysts. *Catal. Today* **2016**, *261*, 60–66.

(11) Guczi, L.; Hoffer, T.; Zsoldos, Z.; Zyade, S.; Maire, G.; Garin, F. Structure and Catalytic Activity of Alumina-Supported Platinum-Cobalt Bimetallic Catalysts. 2. Chemisorption and Catalytic Reactions. *J. Phys. Chem.* **1991**, *95*, 802–808.

(12) Schanke, D.; Vada, S.; Blekkan, E. A.; Hilmen, A. M.; Hoff, A.; Holmen, A. Study of Pt-Promoted Cobalt CO Hydrogenation Catalysts. *Fuel Energy Abstr.* **1995**, *156*, 85–95.

(13) Vada, S.; Hoff, A.; Adnanes, E.; Schanke, D.; Holmen, A. Fischer-Tropsch Synthesis on Supported Cobalt Catalysts Promoted by Platinum and Rhenium. *Top. Catal.* **1995**, *2*, 155–162.

(14) Jacobs, G.; Chaney, J. a; Patterson, P. M.; Das, T. K.; Maillot, J. C.; Davis, B. H. Fischer-Tropsch Synthesis: Study of the Promotion of Pt on the Reduction Property of Co/Al2O3 Catalysts by in Situ EXAFS of Co K and Pt LIII Edges and XPS. *J. Synchrotron Radiat.* **2004**, *11*, 414–422.

(15) Wang, H.; Zhou, W.; Liu, J.; Si, R.; Sun, G.; Zhong, M.; Su, H.; Zhao, H.-B.; Rodriguez, J. A.; Pennycook, S. J.; et al. Platinum-Modulated Cobalt Nanocatalysts for Low-Temperature Aqueous-Phase Fischer-Tropsch Synthesis. *J. Am. Chem. Soc.* **2013**, *135*, 4149–4158.

(16) Gnanamani, M. K.; Ribeiro, M. C.; Ma, W.; Shafer, W. D.; Jacobs, G.; Graham, U. M.; Davis, B. H. Fischer-Tropsch Synthesis: Metal-Support Interfacial Contact Governs Oxygenates Selectivity over CeO2 Supported Pt-Co Catalysts. *Appl. Catal. A Gen.* **2011**, *393*, 17–23.

(17) O'Neill, B. J.; Jackson, D. H. K.; Lee, J.; Canlas, C.; Stair, P. C.; Marshall, C. L.; Elam, J. W.; Kuech, T. F.; Dumesic, J. A.; Huber, G. W. Catalyst Design with Atomic Layer Deposition. *ACS Catal.* **2015**, *5*, 1804–1825.

(18) Singh, J. A.; Yang, N.; Bent, S. F. Nanoengineering Heterogeneous Catalysts by Atomic Layer Deposition. *Annu. Rev. Chem. Biomol. Eng.* **2017**, *8*, 41–62.

(19) Camacho-Bunquin, J.; Shou, H.; Aich, P.; Beaulieu, D. R.; Klotzsch, H.; Bachman, S.;

Marshall, C. L.; Hock, A.; Stair, P. Catalyst Synthesis and Evaluation Using an Integrated Atomic Layer Deposition Synthesis–catalysis Testing Tool. *Rev. Sci. Instrum.* **2015**, *86*, 84103.

(20) Liang, X.; Lyon, L. B.; Jiang, Y.-B.; Weimer, A. W. Scalable Synthesis of Palladium Nanoparticle Catalysts by Atomic Layer Deposition. *J. Nanoparticle Res.* **2012**, *14*, 1–12.

(21) Gould, T. D.; Montemore, M. M.; Lubers, A. M.; Ellis, L. D.; Weimer, A. W.; Falconer, J. L.; Medlin, J. W. Enhanced Dry Reforming of Methane on Ni and Ni-Pt Catalysts Synthesized by Atomic Layer Deposition. *Appl. Catal. A Gen.* **2015**, *492*, 107–116.

(22) Singh, J. A.; Thissen, N. F. W.; Kim, W.-H.; Johnson, H.; Kessels, W. (Erwin) M. .; Bol, A. A.; Bent, S. F.; Mackus, A. J. M. Area-Selective Atomic Layer Deposition of Metal Oxides on Noble Metals through Catalytic Oxygen Activation. *Chem. Mater.* **2017**, acs.chemmater.7b03818.

(23) Cronauer, D. C.; Elam, J. W.; Kropf, A. J.; Marshall, C. L.; Gao, P.; Hopps, S.; Jacobs, G.; Davis, B. H. Fischer–Tropsch Synthesis: Preconditioning Effects Upon Co-Containing Promoted and Unpromoted Catalysts. *Catal. Letters* **2012**, *142*, 698–713.

(24) Libera, J. A.; Elam, J. W.; Pellin, M. J. Conformal ZnO Coatings on High Surface Area Silica Gel Using Atomic Layer Deposition. *Thin Solid Films* **2008**, *516*, 6158–6166.

(25) Kumar, N.; Jothimurugesan, K.; Stanley, G. G.; Schwartz, V.; Spivey, J. J. In Situ FT-IR Study on the Effect of Cobalt Precursors on CO Adsorption Behavior. *J. Phys. Chem. C* **2011**, *115*, 990–998.

(26) Giannozzi, P.; Baroni, S.; Bonini, N.; Calandra, M.; Car, R.; Cavazzoni, C.; Ceresoli, D.;

Chiarotti, G. L.; Cococcioni, M.; Dabo, I.; et al. QUANTUM ESPRESSO: A Modular and Open-Source Software Project for Quantum Simulations of Materials. *J. Phys. Condens. Matter* **2009**, *21*, 395502.

(27) Pack, J. D.; Monkhorst, H. J. "Special Points for Brillouin-Zone Integrations"—a Reply. *Phys. Rev. B* **1977**, *16*, 1748–1749.

(28) Wellendorff, J.; Lundgaard, K. T.; Møgelhøj, A.; Petzold, V.; Landis, D. D.; Nørskov, J. K.; Bligaard, T.; Jacobsen, K. W. Density Functionals for Surface Science: Exchange-Correlation Model Development with Bayesian Error Estimation. *Phys. Rev. B - Condens. Matter Mater. Phys.* **2012**, *85*, 32–34.

(29) Wellendorff, J.; Lundgaard, K. T.; Jacobsen, K. W.; Bligaard, T. mBEEF: An Accurate Semi-Local Bayesian Error Estimation Density Functional. *J. Chem. Phys.* **2014**, *140*, 144107.

(30) Bahn, S. R.; Jacobsen, K. W. An Object-Oriented Scripting Interface to a Legacy Electronic Structure Code. *Comput. Sci. Eng.* **2002**, *4*, 56–66.

(31) Ducreux, O.; Rebours, B.; Lynch, J.; Roy-Auberger, M.; Bazin, D. Microstructure of Supported Cobalt Fischer-Tropsch Catalysts. *Oil Gas Sci. Technol. - Rev. l'IFP* **2009**, *64*, 49–62.

(32) Ming, H.; Baker, B. Characterization of Cobalt Fischer-Tropsch Catalysts I. Unpromoted Cobalt-Silica Gel Catalysts. *Appl. Catal. A Gen.* **1995**, *123*, 23–36.

(33) Lopez, L.; Velasco, J.; Montes, V.; Marinas, A.; Cabrera, S.; Boutonnet, M.; Järås, S. Synthesis of Ethanol from Syngas over Rh/MCM-41 Catalyst: Effect of Water on Product

Selectivity. *Catalysts* **2015**, *5*, 1737–1755.

(34) Kapteijn, F.; Berger, R. J.; Moulijn, J. A. Macrokinetics and Transport Processes. *Handb. Heterog. Catal.* **2008**, *1*, 1693–1714.

(35) Schumann, J.; Lunkenbein, T.; Tarasov, A.; Thomas, N.; Schlögl, R.; Behrens, M. Synthesis and Characterisation of a Highly Active Cu/ZnO:Al Catalyst. *ChemCatChem* **2014**, *6*, 2889–2897.

(36) van den Berg, R.; Prieto, G.; Korpershoek, G.; van der Wal, L. I.; van Bunningen, A. J.; Lægsgaard-Jørgensen, S.; de Jongh, P. E.; de Jong, K. P. Structure Sensitivity of Cu and CuZn Catalysts Relevant to Industrial Methanol Synthesis. *Nat. Commun.* **2016**, *7*, 13057.

(37) Studt, F.; Behrens, M.; Kunkes, E. L.; Thomas, N.; Zander, S.; Tarasov, A.; Schumann, J.; Frei, E.; Varley, J. B.; Abild-Pedersen, F.; et al. The Mechanism of CO and CO2 Hydrogenation to Methanol over Cu-Based Catalysts. *ChemCatChem* **2015**, *7*, 1105–1111.

(38) Bravo-Suárez, J. J.; Chaudhari, R. V.; Subramaniam, B. Design of Heterogeneous Catalysts for Fuels and Chemicals Processing: An Overview BT - Novel Materials for Catalysis and Fuels Processing. *Nov. Mater. Catal. Fuels Process.* **2013**, *1132*, 3–68.

(39) Fenske, D.; Yim, W. L.; Neuendorf, S.; Hoogestraat, D.; Greshnykh, D.; Borchert, H.; Klüner, T.; Al-Shamery, K. Pitfalls in Interpreting Temperature Programmed Desorption Spectra of Alloys: The CO/CoPt Puzzle. *ChemPhysChem* **2007**, *8*, 654–656.

(40) Song, D.; Li, J.; Cai, Q. In Situ Diffuse Reflectance FTIR Study of CO Adsorbed on a Cobalt Catalyst Supported by Silica with Different Pore Sizes. *J. Phys. Chem. C* **2007**,

111, 18970–18979.

(41) Smith, M. L.; Kumar, N.; Spivey, J. J. CO Adsorption Behavior of Cu/SiO2 , Co/SiO2 , and CuCo/SiO2 Catalysts Studied by in Situ DRIFTS. *J. Phys. Chem. C* **2012**, *116*, 7931–7939.

(42) Zhang, M.; Zhang, W.; Xie, W.; Qi, Z.; Wu, G.; Lv, M.; Sun, S.; Bao, J. Effects of Cobalt Promoter and Reduction Temperature on the Surface Species and Syngas Adsorption of K–Co–Mo/C Catalyst for Mixed Alcohols Synthesis. *J. Mol. Catal. A Chem.* **2014**, *395*, 269–275.

(43) Khodakov, A. Y.; Lynch, J.; Bazin, D.; Rebours, B.; Zanier, N.; Moisson, B.; Chaumette, P. Reducibility of Cobalt Species in Silica-Supported Fischer–Tropsch Catalysts. *J. Catal.* **1997**, *168*, 16–25.

(44) Couble, J.; Bianchi, D. Heats of Adsorption of Linearly Adsorbed CO Species on Co2+ and Co0 Sites of Reduced Co/Al2O3 Catalysts in Relationship with the CO/H2 Reaction. *Appl. Catal. A Gen.* **2012**, *445–446*, 1–13.

(45) Heal, M. J.; Leisegang, E. C.; Torrington, R. G. Infrared Studies of Carbon Monoxide and Hydrogen Adsorbed on Silica-Supported Iron and Cobalt Catalysts. *J. Catal.* **1978**, *51*, 314–325.

(46) Weststrate, C. J.; van de Loosdrecht, J.; Niemantsverdriet, J. W. Spectroscopic Insights into Cobalt-Catalyzed Fischer-Tropsch Synthesis: A Review of the Carbon Monoxide Interaction with Single Crystalline Surfaces of Cobalt. *J. Catal.* **2016**, *342*, 1–16.

(47) Kadinov, G.; Bonev, C.; Todorova, S.; Palazov, A. IR Spectroscopy Study of CO

Adsorption and of the Interaction between CO and Hydrogen on Alumina-Supported Cobalt. *J. Chem. Soc. Faraday Trans.* **1998**, *94*, 3027–3031.

(48) Kumar, N.; Smith, M. L.; Spivey, J. J. Characterization and Testing of Silica-Supported Cobalt-Palladium Catalysts for Conversion of Syngas to Oxygenates. *J. Catal.* **2012**, *289*, 218–226.

(49) Yang, N.; Yoo, J. S.; Schumann, J.; Bothra, P.; Singh, J. A.; Valle, E.; Abild-Pedersen, F.; Nørskov, J. K.; Bent, S. F. Rh-MnO Interface Sites Formed by Atomic Layer Deposition Promote Syngas Conversion to Higher Oxygenates. *ACS Catal.* **2017**, *7*, 5746–5757.

(50) Yoshida, H.; Ogawa, K.; Todoroki, N.; Yamada, Y.; Wadayama, T. Carbon Monoxide Adsorption on Cobalt-Deposited Platinum Single Crystal Surfaces Investigated by IR Reflection-Absorption and Low-Energy Electron Diffraction. *e-Journal Surf. Sci. Nanotechnol.* **2010**, *8*, 161–166.

(51) Kappers, M. J.; van der Maas, J. H. Correlation between CO Frequency and Pt Coordination Number. A DRIFT Study on Supported Pt Catalysts. *Catal. Letters* **1991**, *10*, 365–373.

(52) Lundwall, M. J.; McClure, S. M.; Goodman, D. W. Probing Terrace and Step Sites on Pt Nanoparticles Using CO and Ethylene. *J. Phys. Chem. C* **2010**, *114*, 7904–7912.

(53) Tong, Y. Y.; Billy, J.; Renouprez, A. J.; van der Klink, J. J. Correlation between the Stretching Frequency of Carbon Monoxide Adsorbed and the Fermi Level Local Density of States at Surfaces of Platinum Catalysts. *J. Am. Chem. Soc.* **1997**, *119*, 3929–3934.

(54) de Menorval, L.-C.; Chaqroune, A.; Coq, B.; Figueras, F. Characterization of Mono- and

Bi-Metallic Platinum Catalysts Using CO FTIR Spectroscopy Size Effects and Topological Segregation. *J. Chem. Soc. Faraday Trans.* **1997**, *93*, 3715–3720.

(55) Blyholder, G. Molecular Orbital View of Chemisorbed Carbon Monoxide. *J. Phys. Chem. A* **1964**, *68*, 2772–2777.

(56) Chandler, B. D.; Pignolet, L. H. DRIFTS Studies of Carbon Monoxide Coverage on Highly Dispersed Bimetallic Pt-Cu and Pt-Au Catalysts. *Catal. Today* **2001**, *65*, 39–50.

(57) Dees, M. J.; Shido, T.; Iwasawa, Y.; Ponec, V. Infrared Studies of Co Adsorbed on Supported Pt Co Catalysts. *J. Catal.* **1990**, *124*, 530–540.

(58) Ruban, A.; Skriver, H.; Nørskov, J. Surface Segregation Energies in Transition-Metal Alloys. *Phys. Rev. B* **1999**, *59*, 15990–16000.

(59) Xin, H. L.; Alayoglu, S.; Tao, R.; Genc, A.; Wang, C.-M.; Kovarik, L.; Stach, E. A.; Wang, L.; Salmeron, M.; Somorjai, G. A.; et al. Revealing the Atomic Restructuring of Pt–Co Nanoparticles. *Nano Lett.* **2014**, *14*, 3203–3207.

(60) Xu, X.-C.; Su, J.; Tian, P.; Fu, D.; Dai, W.; Mao, W.; Yuan, W.; Xu, J.; Han, Y. First-Principles Study of C 2 Oxygenates Synthesis Directly from Syngas over CoCu Bimetallic Catalysts. *J. Phys. Chem. C* **2015**, *119*, 216–227.

(61) Choi, Y.; Liu, P. Mechanism of Ethanol Synthesis from Syngas on Rh(111). *J. Am. Chem. Soc.* **2009**, *131*, 13054–13061.

(62) Yang, N.; Medford, A. J.; Liu, X.; Studt, F.; Bligaard, T.; Bent, S. F.; Norskov, J. K. Intrinsic Selectivity and Structure Sensitivity of Rhodium Catalysts for C2+ Oxygenate Production. *J. Am. Chem. Soc.* **2016**, *138*, 3705–3714.

(63) Luk, H. T.; Mondelli, C.; Ferré, D. C.; Stewart, J. A.; Pérez-Ramírez, J. Status and Prospects in Higher Alcohols Synthesis from Syngas. *Chem. Soc. Rev.* **2017**, *46*, 1358–1426.

(64) Tsubaki, N.; Sun, S.; Fujimoto, K. Different Functions of the Noble Metals Added to Cobalt Catalysts for Fischer-Tropsch Synthesis. *J. Catal.* **2001**, *199*, 236–246.

(65) Gopalakrishnan, R.; Viswanathan, B. Temperature-Programmed Desorption and Infrared Studies on the Activation of Carbon Monoxide on Cobalt Surfaces. *J. Colloid Interface Sci.* **1984**, *102*, 370–372.

(66) Zhu, H.; Wu, Z.; Su, D.; Veith, G. M.; Lu, H.; Zhang, P.; Chai, S.-H.; Dai, S. Constructing Hierarchical Interfaces: TiO 2 -Supported PtFe–FeO X Nanowires for Room Temperature CO Oxidation. *J. Am. Chem. Soc.* **2015**, *137*, 10156–10159.

(67) Baschuk, J. J.; Li, X. Carbon Monoxide Poisoning of Proton Exchange Membrane Fuel Cells. *Int. J. Energy Res.* **2001**, *25*, 695–713.

(68) Pei, Y.-P.; Liu, J.-X.; Zhao, Y.-H.; Ding, Y.-J.; Liu, T.; Dong, W.-D.; Zhu, H.-J.; Su, H.-Y.; Yan, L.; Li, J.-L.; et al. High Alcohols Synthesis via Fischer–Tropsch Reaction at Cobalt Metal/Carbide Interface. *ACS Catal.* **2015**, *5*, 3620–3624.

(69) Song, X.; Ding, Y.; Chen, W.; Dong, W.; Pei, Y.; Zang, J.; Yan, L.; Lu, Y. Synthesis and Characterization of Silica-Supported Cobalt Phosphide Catalysts for CO Hydrogenation. *Energy and Fuels* **2012**, *26*, 6559–6566.

TOC Graphic